Mechanism of reductive fluorination by PTFE-decomposition fluorocarbon gases for WO_3

Hiroki Yamamoto,[1,2] Kohei Tada,[2] Jinkwang Hwang,[1] Daigorou Hirai,[3]

Zenji Hiroi,[3] Kazuhiko Matsumoto,[1*] Rika Hagiwara[1]

[1] *Graduate School of Energy Science, Kyoto University, Yoshida, Sakyo-ku, Kyoto 606-8501, Japan*

[2] *Research Institute of Electrochemical Energy (RIECEN), National Institute of Advanced Industrial Science and Technology (AIST), 1-8-31 Midorigaoka, Ikeda, Osaka 563-8577, Japan*

[3] *Institute for Solid State Physics, The University of Tokyo, Kashiwa, Chiba 277-8581, Japan*

**Corresponding author*. Tel: +81-75-753-4817. E-mail: k-matsumoto@energy.kyoto-u.ac.jp (K. Matsumoto)

†Supplementary information (S.I.) available: xxxxxxxxxxxxxxx. See DOI: xxxxxxxxxx

ABSTRACT.

Reductive fluorination, which entails the substitution of O^{2-} from oxide compounds with F^- from fluoropolymers, is considered a practical approach for preparing transition-metal oxyfluorides. However, the current understanding of the fundamental reaction paths remains limited due to the analytical complexities posed by high-temperature reactions in glassware. Therefore, to expand this knowledgebase, this study investigates the reaction mechanisms behind the reductive fluorination of WO_3 using polytetrafluoroethylene (PTFE) in a Ni reactor. Here, we explore varied reaction conditions (temperature, duration, and F/W ratio) to suppress the formation of carbon byproducts, minimize the dissipation of fluorine-containing tungsten (VI) compounds, and achieve a high fluorine content. The gas-solid reaction paths are analyzed using infrared spectroscopy which revealed tetrafluoroethylene (C_2F_4), hexafluoropropene (C_3F_6), and iso-octafluoroisobutene (*i*-C_4F_8) to be the reactive components in the PTFE-decomposition gas during the reactions with WO_3 at 500 °C. CO_2 and CO are further identified as gaseous byproducts of the reaction evincing that the reaction is prompted by difluorocarbene ($:CF_2$) formed after the cleavage of C=C bonds in *i*-C_4F_8, C_3F_6, and C_2F_4 upon contact with the WO_3 surface. The solid-solid reaction path is established through a reaction between WO_3 and $WO_{3-x}F_x$ where solid-state diffusion of O^{2-} and F^- is discerned at 500 °C.

1. INTRODUCTION

Transition-metal oxides have gained widespread utility as multi-functional materials on the grounds of their ubiquity and chemical, structural and electronic functionalities that facilitate the uses as catalysis, energy materials, and even next-generation electronics.[1-3] Moreover, their oxide frameworks allow the introduction of different anionic species to form mixed anion compounds, some of which have been noted to have vastly disparate properties.[4-12] For transition-metal compounds, the valence states and electronic properties of the central atoms are influenced by the surrounding anions, and thus modifying the anions even in non-stoichiometric amounts, can generate new properties. Prime examples of such compounds are oxyfluorides which are formed through the substitution of O^{2-} anions with F^{-} anions. Since fluorine has one proton and electron more than oxygen, the anion substitution introduces an additional electron into the conduction bands of the parent compound – a mechanism that has been linked to increased conductivities in some of the transition-metal oxyfluorides reported. This advantage of F^{-} anion modification is further complemented by the similarity in the ionic sizes of the F^{-} and O^{2-} anions which minimize the structural deformation during the process.[4,6,13-22]

Fluorination techniques have become subjects of interest in recent studies focusing

on oxyfluorides. Although various fluorinating reagents such as elemental F_2, HF, and SF_4 have been reported, most of them tend to be oxidative or substitutive. In addition, these reagents are highly toxic and corrosive, which makes them difficult to handle. As a solution, fluoropolymers such as polytetrafluoroethylene (PTFE)[13-15,23-30] or polyvinylidene difluoride[15,31-36]has drawn interest. This fluorination technique facilitates the simultaneous exchange of the O^{2-} from the transition-metal oxides and the F^{-} from the fluorocarbon gases while reducing the oxidation state of the central atom. In particular, PTFE has been adapted for the reductive fluorination of transition-metal oxides such as Nb_2O_5, Ta_2O_5, and MoO_3, whereby the degree of fluorination and the resultant oxyfluoride structures can be controlled by adjusting the quantity of PTFE employed or varying the reaction temperatures.[13]

Among the transition-metal oxides investigated so far, reductive fluorination is particularly suited for WO_3 – a material of focus in both experimental and theoretical researches.[14,23,37-42] WO_3 has been found to undergo complicated structural evolutions when subjected to certain conditions. For instance, when heat is applied, the low-temperature monoclinic (II) phase transforms into a monoclinic (I) phase via a triclinic structure. The monoclinic (I) phase, which is stable at room temperature, transforms into an orthorhombic phase when heated to around 330 °C, after which it changes to a

tetragonal phase.[43,44] Likewise, substituting the O^{2-} in WO_3 with F^- has been found to form $WO_{3-x}F_x$–type fluorinated WO_3 with different structural configurations depending on the amount of F. Previous studies have shown that fluorinating WO_3 using PTFE produces a $WO_{3-x}F_x$ whose structure changes from a monoclinic lattice to orthorhombic, tetragonal, and cubic ones with increasing degrees of fluorination.[14,23,37-39] The benefits of high degrees of fluorination are represented by the cubic phase of $WO_{3-x}F_x$ (x = 0.45), which manifests superconducting properties and significantly smaller resistivity compared with WO_3 and the tetragonal phase of $WO_{3-x}F_x$ (x = 0.11).[14] The efficacy of reductive fluorination was confirmed by a study that achieved a highly fluorinated $WO_{3-x}F_x$ (x = 0.60) through spark plasma sintering a mixture of WO_3 and PTFE powder, which provided photocatalytic properties.[23] It is worth noting that the resulting $WO_{3-x}F_x$ (x = 0.60) was comparable to a previous x = 0.66 product achieved through fluorination using HF under extreme conditions: 3000 atm and 700 °C in a sealed gold ampoule.[37] XPS spectroscopy also revealed the $WO_{3-x}F_x$ synthesized using PTFE comprised W atoms with the mixed oxidation states of +6 and +5.[23]

The pivotal role of PTFE in reductive fluorination has led to numerous investigations into its decomposition behavior under different conditions.[45-65] According to previous work, the decomposition of PTFE generally starts around 260 °C and significantly

escalates over 400 °C.[48] From a chemical perspective, the decomposition process begins after the C–C bonds in PTFE are broken, leading to the formation of difluorocarbene ($:CF_2$). Subsequently, various fluorocarbon gases such as tetrafluoroethylene (C_2F_4), perfluorocyclobutane (c-C_4F_8), hexafluoropropene (C_3F_6), octafluoroisobutene (i-C_4F_8), and hexafluoroethane (C_2F_6) are formed depending on atmospheres and temperatures.[45,46] Regarding the roles of these decomposition products in reductive fluorination, some reports have suggested that the process is mainly induced by C_2F_4 to form CO_2.[15,23] Despite the knowledge amassed on the subject, the correlation between the decomposition products from PTFE and the reductive fluorination of transition-metal oxides such as WO_3 has not been verified to the best of our knowledge. As such, this study attempts to elucidate the underlying reaction mechanism between WO_3 and PTFE-decomposition gas. Besides the gas-solid reactions, a solid-solid reaction between WO_3 and $WO_{3-x}F_x$ was also conducted to affirm the mutual diffusion of F^- and O^{2-} in the solid state.

2. EXPERIMENTAL SECTION

Apparatus and materials. All volatile materials were handled in a reaction manifold made of SUS-316 stainless steel and tetrafluoroethylene-perfluoroalkylvinylether copolymer.[66] The gaseous materials in the reaction manifold were evacuated through a

soda lime chemical trap, and thereafter, a cold trap cooled to −196 °C by liquid nitrogen. The non-volatile materials were, when necessary, handled under a dry Ar atmosphere in a glove box. A Ni reactor (100 cm^3) equipped with a corrosion-resistant valve was used for reactions. The reactor lid was air-cooled during reactions. A tube made of CaF_2 crystal was used for infrared (IR) measurements of PTFE-decomposition gas at 500 °C. Additional details of the measurement methods will be provided in the next subsection. Approximately 100 mg of WO_3 powder (FUJIFILM Wako Chemicals, mean diameter ~100 nm) was pressed into a pellet with a diameter of 6 mm and a thickness of 0.7 mm (~30% porosity). PTFE powder (FUJIFILM Wako Chemicals, MW 5,000~20,000) was used as purchased.

Analyses. Infrared spectra of gaseous samples were recorded using an ALPHA II spectrometer (Bruker Optics Laboratories, Inc.) in the transmission mode with the aid of a gas cell with AgCl windows. Powder X-ray diffraction (XRD) patterns were obtained in a Bragg-Brentano geometry using a Smartlab diffractometer (Rigaku Corp., D-tex Ultra 250) equipped with a Si-strip high-speed detector (Cu *K*α radiation, 40 kV-30 mA). X-ray photoelectron spectroscopy (XPS) data were obtained with a JPS-9030 MC spectrometer (JEOL, Ltd., MgKα radiation). The samples for XPS analysis were fixed on

indium metal foil. The baseline was corrected by the Shirley method and fitting of the resulting spectrum was performed using pseudo Voigt function. Thermal stability of the sample was investigated by a thermogravimetric differential thermal analyzer (ThermoPlusEvo2 TG8120) at a scan rate of 5 °C min^{-1} under an Ar flow atmosphere. The sample for thermogravimetry was loaded on an Al pan. Elemental analysis was performed Organic Microanalysis Laboratory, Kyoto University. Carbon content was analyzed by combustion analysis (J-Science Lab JM11). Fluorine content was analyzed by ion chromatography (ThermoFisher ICS-1600) after complete combustion. The F content by this method was validated by comparing several obtained values with the ones by the fluoride ion selective electrode method.[67]

Decomposition behavior of PTFE under vacuum at different decomposition and measurement temperatures. The decomposition gases of PTFE were analyzed by IR measurements at 25 °C and 500 °C. For the IR measurements at 500 °C, a stainless-steel block with a horizontal through-hole and a vertical blind hole was placed in the IR spectrometer within the confines of the glove box. The outside of the heating block was cooled with blown Ar to avoid damaging the spectrometer. The tube made of CaF_2 was placed in the vertical blind hole and gradually heated up to 500 °C using a heater built

into the stainless-steel block. The PTFE powder, dried overnight under vacuum at 150 °C, was placed in the CaF_2 tube, whereafter, the IR spectrum of the decomposition gas was immediately obtained. For the IR measurements at 25 °C, PTFE powder on a Ni boat was loaded into the Ni reactor. The Ni reactor was heated to 150 °C under vacuum overnight to dry the PTFE powder. The reactor was then isolated from the reaction manifold and heated to the respective target temperatures (450, 500, or 550 °C) for more than 12 h. After the PTFE decomposition, the Ni reactor was cooled to 25 °C overnight. The volatile gas was subsequently transferred to a gas cell for IR measurements.

One-step reactions of WO_3 with PTFE-decomposition gases. A WO_3 pellet (approximately 100 mg) and PTFE powder (F/W = 3.56, 6.00, 8.00, 10.00, or 12.00; where F/W is the molar ratio of the F in PTFE ($(C_2F_4)_n$) to the W in WO_3) were loaded onto separate Ni boats and placed inside the Ni reactor. The reactor was heated to 150 °C under vacuum overnight to dry the starting materials. The reactor was subsequently isolated from the reaction manifold and heated to the respective target temperatures (450, 500, or 550 °C) for designated durations (4, 12, or 36 h). After each reaction, the reactor was cooled to 25 °C overnight, whereafter the volatile gas was transferred to the gas cell for IR measurements and the solid product was isolated for further analyses. Caution:

Fluorocarbon gases formed by PTFE decomposition are hazardous and must be carefully handled to prevent any exposures.[45]

Two-step reaction of WO_3 with PTFE-decomposition gases. For this investigation, two Ni reactors were employed to separate the reaction between WO_3 and PTFE decomposition gases. One reactor loaded with PTFE powder on a Ni boat was used for PTFE decomposition (F/W = 8.00). The other reactor enclosed the WO_3 pellet on a Ni boat and was used the reaction between the PTFE decomposition gas and WO_3. Both the reactors were heated to 150 °C under vacuum overnight to dry the starting materials and isolated from the reaction manifold. The PTFE-decomposition process was conducted at 500 °C for 12 h, after which the Ni reactor was cooled to 25 °C overnight. A portion of the volatile gas was transferred to the gas cell for IR measurements to ascertain the gas components. Subsequently, the volatile gases both in the first Ni reactor and in the gas cell were entirely transferred to the second Ni reactor containing WO_3 by cooling it to −196 °C using liquid nitrogen. After the gas transfer, the second reactor was isolated from the reaction manifold and heated to 500 °C for 36 h. Once the reaction was complete, the reactor was cooled down to 25 °C overnight. The volatile gas was transferred to the gas cell for IR measurements, and the solid product was isolated for further analyses.

Solid-solid reaction of WO_3 and $WO_{3-x}F_x$. WO_3 and $WO_{3-x}F_x$ (x = 0.36, synthesized by the reaction of WO_3 and PTFE at 500 °C for 36 h with the F/W ratio of 6.00 as described in Table 1) powders were mixed using a pestle and a mortar and pressed into a pellet. The obtained pellet was placed on a Ni boat and loaded into the Ni reactor for drying under vacuum at 150 °C overnight. The reactor was isolated from the reaction manifold and heated to 500 °C for 24 h. After the reaction, the Ni reactor was cooled down to 25 °C, and the solid product was isolated for further analyses.

Quantum chemical calculations. Theoretical calculations were performed based on density functional theory (DFT) and Møller-Plesset perturbation theory (MP). The exchange-correlation functional for DFT was B3LYP[68], and the 2nd order perturbation was adopted for MP (MP2 method).[69] The calculations were performed using the Gaussian16 program.[70] The total energies, electronic structures, and bond frequencies of C_2H_4, $:CF_2$, C_2F_4, C_3F_6, *i*-C_4F_8, 1-octafluorobutene (1-C_4F_8), 2-*cis*-octafluorobutene (2-*cis*-C_4F_8), and 2-*trans*-octafluorobutene (2-*trans*-C_4F_8) were estimated using the 6-311+G(d,p) basis set. The optimized geometries had no imaginary frequency. Wiberg bond indices were calculated as the bond orders via the natural atomic orbital analysis

71,72

3. RESULTS AND DISCUSSION

Reactions of WO_3 with PTFE-decomposition gases at different conditions. In the present study, Ni reactors were selected for reductive fluorination reactions due to their low reactivity with PTFE-decomposition gases, which provides higher durability than quartz reactors (see Supporting Information for the IR spectra (Figure S1) and additional discussion on the PTFE-deposition gas reactivity with quartz at 550 °C). As shown by the schematic in Figure 1(a), the WO_3 and PTFE samples were loaded onto separate boats in the same Ni reactor heated in a one-step reaction process. Table 1 highlights the reaction parameters *i.e.*, temperature, duration, and F/W ratio (elemental ratio of F in PTFE ($(C_2F_4)_n$) to W in WO_3) alongside data derived from the reaction products (R_w (wt%): weight of $WO_{3-x}F_x$ after reaction/weight of WO_3 before reaction; C_F (wt%): fluorine content in products; x: composition of $WO_{3-x}F_x$ calculated from C_F; and C_c (wt%): carbon content in products).

The effect of temperature on the reactivity was investigated by comparing the reaction products obtained under different reaction temperatures with the reaction duration and F/W ratio parameters (36 h and F/W = 3.56) kept constant. A reaction temperature of

550 °C was selected to compare the reaction products to those obtained by a previous study that utilized a quartz reactor.[14] At that temperature, the reaction product have a C_F of 3.41 % ($WO_{2.58}F_{0.42}$), which is comparable to the $WO_{2.55}F_{0.45}$ previously reported. The product had a low R_w of 25.3% despite the high fluorine content. The large decrease in weight indicates that the fluorinated product partially sublimed as was confirmed by the presence of fluorine-containing tungsten species around the lid (cooler parts) of the Ni reactor. On the other hand, the reaction product in the Ni boat was found to have a high C_c of 3.87 %, revealing that the reaction between the PTFE-decomposition gas and WO_3 at 550 °C forms carbon byproduct – consistent with the black color of the product. The structure of this residual carbon was analyzed by XRD in the case of the reaction with excess PTFE (F/W = 54.2) at 550 °C which gave a high carbon content of 73.7 %. The resulting XRD pattern indicates its amorphous structure characterized by broad peaks around 23° and 42° corresponding to 002 and 100 diffraction lines, respectively (see Figure S2 for the corresponding XRD pattern). The solubility of carbon into the $WO_{3-x}F_x$ host is neglected in the following characterization.

Further, the reaction product attained at 450 °C (36 h and F/W = 3.56) was investigated to ascertain the effect of lower reaction temperatures. Here, the sublimation of $WO_{3-x}F_x$ and the carbon formed were significantly suppressed, yielding a high R_w of 98.3% and a

low C_c of 0.15%. Even so, the reaction yielded a lower fluorine content (C_F of 0.22 % corresponding to $WO_{2.97}F_{0.03}$), signifying that the low reaction temperature was not sufficient to complete the PTFE decomposition; as corroborated by the residual PTFE, which had melted and resolidified in the Ni boat in the course of the reaction. This product (450 °C) was light blue and was comparable to a previously reported product with a low fluorination degree (light green for x = 0.04 (orthorhombic structure)).[37] In an attempt to increase the fluorination degree, reaction products from the higher reaction temperature of 500 °C (36 h and F/W = 3.56) were examined. The fluorinated product was dark blue with a higher R_w of 76.8 %, a slightly lower C_F of 2.94 % ($WO_{2.64}F_{0.36}$), and a significantly lower C_c of 0.32 wt%, compared to the product obtained at 550 °C. Thermogravimetric analysis revealed that $WO_{2.64}F_{0.36}$ has a high thermal stability, exhibiting a gentle weight loss up to 500 °C (1% and 5% weight loss at 195 °C and >500 °C, respectively) (see Figure S3 for the thermogravimetric curve of $WO_{2.64}F_{0.36}$). The presence of W^{5+} in $WO_{2.64}F_{0.36}$ is confirmed by XPS analysis (see Figures S4 for XPS spectrum of $WO_{2.64}F_{0.36}$). The W^{6+}/W^{5+} ratio estimated by peak fitting is consistent with the composition of $WO_{2.64}F_{0.36}$ (W^{6+}/W^{5+} = 0.64/0.36), suggesting the negligible contribution of anionic vacancy which can affect the W^{6+}/W^{5+} ratio.

Table 1. Experimental conditions and results of the reactions between WO_3 and the PTFE-decomposition gas

Entry	Temperature [°C]	F/W [a]	Time [h]	R_w [b] [wt%]	C_F [c] [wt%]	Composition x in $WO_{3-x}F_x$ [d]	C_C [e] [wt%]	Product color
1	450	3.56	36	98.3	0.22	0.03	0.15	Light blue
2	500	3.56	4	92.9	1.36	0.17	< 0.10	Blue
3	500	3.56	12	92.6	1.46	0.18	0.16	Blue
4	500	3.56	36	76.8	2.94	0.36	0.32	Dark blue
5	500	6.00	36	76.9	2.91	0.36	0.16	Dark blue
6	500	8.00	36	76.7	2.58	0.32	0.13	Dark blue
7	500	10.00	36	63.4	3.55	0.44	0.52	Light purple
8	500	12.00	36	41.0	3.49	0.43	2.20	Bluish black
9	550	3.56	36	25.3	3.41	0.42	3.87	Black

[a] F/W: elemental ratio of F in PTFE ($(C_2F_4)_n$) to W in WO_3, [b] R_w: weight of $WO_{3-x}F_x$ (after reaction) / weight of WO_3 (before reaction), [c] C_F: fluorine content in product, [d] the composition x in $WO_{3-x}F_x$ is determined based on C_F, [e] C_C: carbon content in product.

For insight into the effect of temperature on the structural configurations of the fluorinated products, the XRD patterns of the reaction products obtained at 450, 500, and 550 °C, for the reaction duration of 36 h and F/W ratio of 3.56, were compared to pristine WO_3, as shown in Figure 1(b). The pristine WO_3 possesses a monoclinic structure as previously reported according to a Rietveld refinement (see Figure S5 and Table S1 for detailed crystallographic parameters). The reaction product obtained at 500 °C, with a composition of $WO_{2.64}F_{0.36}$ (Table 1), is assigned to a single cubic phase. Rietveld refinement confirmed that this phase belongs to the ReO_3-type structure with O/F-disordering in congruence with a previous report (see Figure S6 and Table S2 for detailed crystallographic parameters).[14,23] At the higher temperature of 550 °C, the reaction yielded a product in the cubic phase. Although some other peaks are also observed in the pattern (around $2\theta = 25.8°$ and 36–38°), they were not able to be indexed as a superlattice by considering the tilting of the octahedra. On the other hand, the XRD pattern of the reaction product obtained at 450 °C only exhibited slight differences from the pristine WO_3 pattern, revealing that the structure is not a cubic phase.

The influence of reaction time was investigated by implementing reactions at the temperature of 500 °C and F/W ratio of 3.56 at varied durations of 4, 12, and 36 h (Table 1). The 4 and 12 h reaction durations yielded products with significantly lower C_F values

(1.36% and 1.46%, respectively) than those obtained in 36 h (2.94%). This XRD analysis confirms that the reaction duration of 36 h is a requisite to achieve a complete transition to the cubic phase (Figure S7 for XRD patterns of the products with different reaction durations). On another note, the PTFE on the Ni boat was observed to completely disappear in all reaction cases. This indicates that even the reaction duration of 4 h was sufficient to facilitate complete PTFE decomposition. These results suggest that the rate-determining step is not the decomposition of PTFE, but rather the reaction between WO_3 and the PTFE-decomposition gas.

The influence of F/W ratio on the reaction between the PTFE-decomposition gas and WO_3 was evaluated by varying the F/W ratio while maintaining the reaction temperature at 500 °C and reaction duration at 36 h. XRD analyses of the reaction products confirmed that the cubic phase was maintained in all the cases regardless of the F/W ratio applied (see Supporting Information; Figure S8 for the XRD patterns of the products with different F/W (3.56, 6.00, 8.00, 10.00, and 12.00) and Figures S9−S12 and Tables S3−S6 for detailed crystallographic parameters by Rietveld refinement). Although only a limited x range is available in the present case, there is a trend that the a lattice parameter increasing with increasing x in $WO_{3-x}F_x$. The correlation between the F/W ratio and the C_F, C_C, and R_w values of the reaction products is summarized in Figure 1(c) (see Table 1

for detailed data). The trend suggests that an increase in the F/W ratio increases the C_F and C_C values and decreases R_w values of the reaction products. Even so, the F/W ratios of over 3.56 did not significantly enhance the F content, but merely accelerated the formation of carbon byproduct and the partial sublimation of the product. The carbon byproduct was visually confirmed by the bluish-black color of the product obtained by F/W = 12.00 (C_C = 2.20 %). The sublimation was corroborated by the color change of the deposits to yellow upon exposure to air around the lid of the Ni reactor, although the large amounts of white repolymerized PTFE from C_2F_4 in the PTFE decomposition gas were also seen when the F/W ratio was increased (see Figure S13 for photos of the lid after the reaction at 500 °C for 36 h with F/W = 12.00).

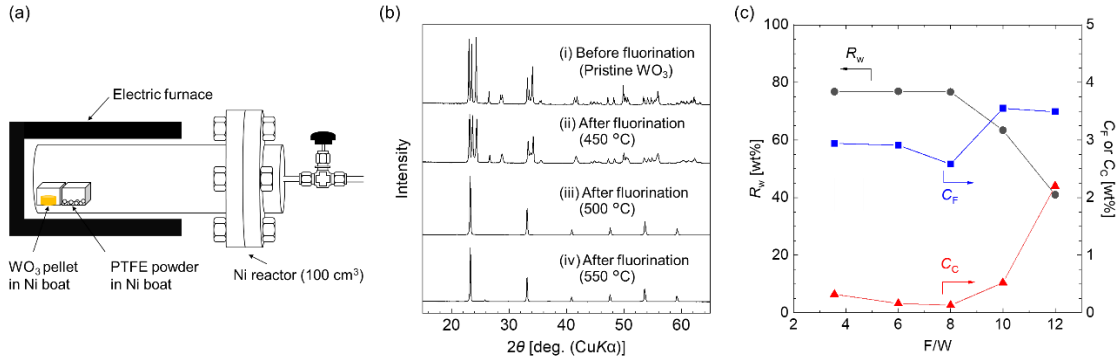

Figure 1. (a) Schematic of the one-step reaction between WO_3 and PTFE. (b) XRD patterns of (i) pristine WO_3 and $WO_{3-x}F_x$ obtained at (ii) 450 °C, (iii) 500 °C, and (iv) 550 °C. The reaction time and F/W ratio were 36 h and 3.56, respectively, in all the cases. See Supporting Information for detailed crystallographic data obtained by Rietveld refinement (Figure S5 and Table S1 for (i) pristine WO_3 and Figure S6 and Table S2 for (iii) $WO_{2.64}F_{0.36}$). (c) The F/W ratio dependency of R_w, C_F, and C_C in reactions of WO_3 and the PTFE-decomposition gas. Reaction temperature: 500 °C and reaction time: 36 h.

PTFE-decomposition gases at different decomposition and measurement temperatures. Identifying the components of the PTFE-decomposition gas is crucial to elucidating the reductive fluorination mechanisms. Indeed, PTFE decomposition has been the subject of many reseasrches,[45-65] which have prescribed the following decomposition mechanism:(i) chain cleavage of PTFE, (ii) :CF_2 formation, (iii) C_2F_4 formation from two :CF_2, (iv-A) *c*-C_4F_8 formation from two C_2F_4 molecules, (iv-B) C_3F_6 formation from C_2F_4 and :CF_2, and (v) *i*-C_4F_8 formation from C_3F_6 and :CF_2.[45,46] It is worth noting that the decomposition mechanism of PTFE is complicated and generally depends on the reaction conditions. In fact, certain conditions have also been reported to generate other chemical species, such as C_2F_6. As such, it is important to investigate mechanism using the present experimental system for clarity.

To determine the components of the PTFE-decomposition gas, IR spectroscopy was performed on the PTFE-decomposition gas produced at 450, 500, and 550 °C; measured after the gas was cooled to 25 °C. A summary of the PTFE-decomposition gas is provided in Table 2. As shown in Figure 2(a-i, ii, and iii), all cases exhibited complicated bands between 1000–1400 cm^{-1}. However, the bands above 1700 cm^{-1} and below 1000 cm^{-1} were clear enough to identify the chemical components of the gas. Each IR spectrum is marked by a band representing the CF_2 symmetric stretching mode of *c*-C_4F_8 at 962

cm^{-1}.[51,73-76] Additionally, the bands appearing at 1751 and 1795 cm^{-1} are ascribed to the C=C stretching mode of *i*-C_4F_8[51,77] and C_3F_6,[51,73,78,79] respectively.

PTFE decomposition at 450 °C gives a gas that mainly consists of *c*-C_4F_8 while C_3F_6 and *i*-C_4F_8 participate as a minor species. When the decomposition temperature was raised to 500 °C, the *i*-C_4F_8 species was seen to increase while the *c*-C_4F_8 and C_3F_6 components decreased. Comparing the intensities of the bands appearing at 962 and 1795 cm^{-1} reveals that decomposition at 500 °C leads to a more significant decrease in the *c*-C_4F_8 than C_3F_6. This trend becomes more prevalent when the temperature is increased to 550 °C, resulting in *i*-C_4F_8 as the main component and *c*-C_4F_8 and C_3F_6 as minor species. It is worth noting that C_2F_4, which is typically represented by a band at 1325 cm^{-1},[51,52] was not identified in the spectra, presumably because it repolymerized back to PTFE when the gas was cooled to 25 °C before the IR spectroscopy. The influence of temperature on the components of the PTFE-decomposition gas aligns with a previous report, although the formation temperatures of the gaseous species were different, probably due to variations in the experimental conditions such as the N_2 flow atmosphere and the sealed quartz reactor used in the previous work.[50]

As mentioned above, the IR spectra obtained after cooling the PTFE-decomposition gases to 25 °C do not entirely reflect the gaseous components involved in the reactions

with WO_3. This deduction is also confirmed by the formation of repolymerized PTFE around the lid of the Ni reactor after the reactions despite the absence of C_2F_4 bands in the IR spectra measured at 25°C. The C_2F_4 gaseous component is particularly difficult to identify at 25 °C due to the formation of overlapping absorption bands and repolymerization. It is interesting to note that although numerous studies have proposed that C_2F_4 is formed immediately after the decomposition of PTFE,[45,46,48,51,52,56] none of them have provided spectroscopic evidence of C_2F_4 at high temperatures of around 500 °C: to the best of our knowledge.

Therefore, for further characterization of the PTFE decomposition components, the gas was subjected to *in situ* IR spectroscopy at 500 °C using a CaF_2 container under a dry Ar atmosphere. The corresponding spectra are illustrated in Figure 2(b). Apart from the broad absorption bands propagated by the high measurement temperature,[73] the *in situ* spectrum displayed other differences from the one measured at 25 °C (Figure 2(a-ii)), even though the decomposition temperature was the same (500 °C). For instance, the characteristic bands corresponding to the C=C stretching modes of C_3F_6 and *i*-C_4F_8, which are expected to appear at 1795 and 1751 cm^{-1}, respectively, are absent in the *in situ* spectrum. Additionally, two broad bands that can be assigned to the CF_2 symmetric and asymmetric stretching modes of C_2F_4 appear at 1000 and 1400 cm^{-1} (reported at 1183 and

1325 cm^{-1} in previous literature).[51,52,73] It is also worth mentioning that the absorption bands for the singlet ground state of :CF_2, which typically appear at 1225 and 1114 cm^{-1} in congruity with the symmetric and asymmetric stretching modes modes[80,81] are not clearly visible in the *in situ* spectrum, although they might still exist as minor components. Nonetheless, the results from this investigation demonstrate that C_2F_4 is formed in the initial step of PTFE decomposition at the high temperature of around 500 °C and further confirm the mechanisms proposed in previous works.[45,46]

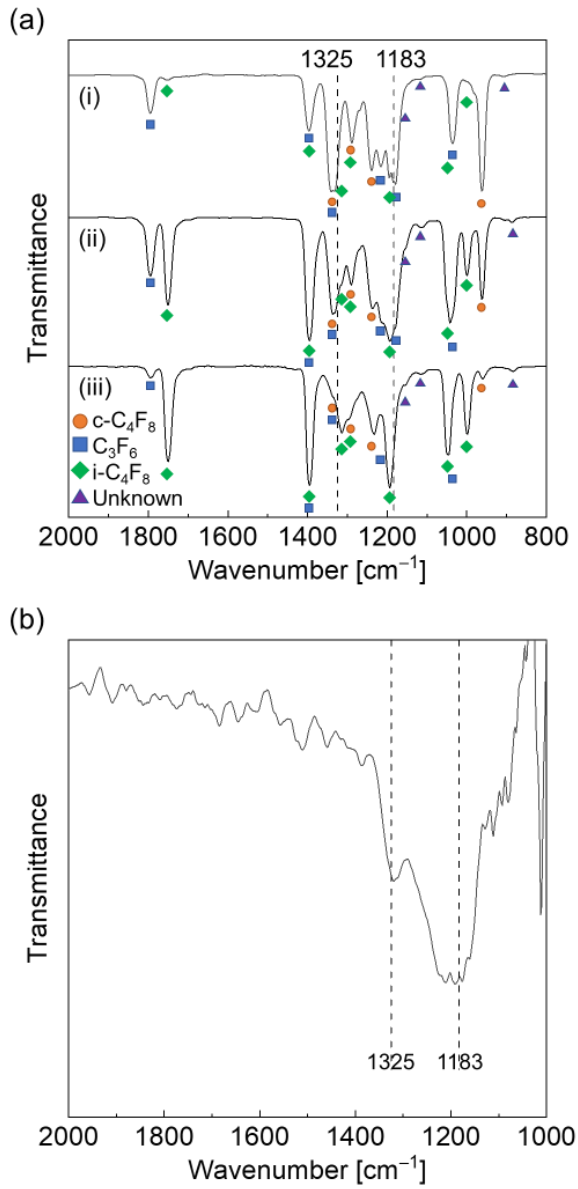

Figure 2. Infrared spectra of PTFE-decomposition gases. (a) Spectra of the gases decomposed at (i) 450 °C, (ii) 500 °C, and (iii) 550 °C (measured after cooling down to 25 °C). (b) *In situ* IR spectrum of the gas decomposed and measured at 500 °C. The wavenumbers of 1183 and 1325 cm^{-1} correspond to the CF_2 symmetric and asymmetric stretching modes of C_2F_4, respectively.[51,52,73] Although the stretching modes of $:CF_2$ may appear in this region (1225 and 1114 cm^{-1} for the singlet ground state of $:CF_2$ according to the literature),[80,81] they are not clearly observed in this spectrum.

Table 2. Components of PTFE-decomposition gases at different decomposition and measurement temperatures

Gaseous species	**Decomposition / measurement temperatures [°C]**			
	450 / 25	500 / 25	550 / 25	500 / 500 (*in situ*)
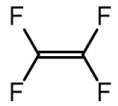 **C_2F_4**	N	N	N	Major
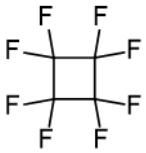 ***c*-C_4F_8**	Major	Secondary	Minor	N
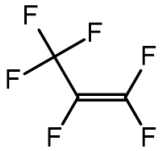 **C_3F_6**	Intermediate	Secondary	Minor	N
 ***i*-C_4F_8**	Minor	Major	Major	N

Major: primary major species, Secondary: secondary major species, Minor: minor species, N: not observed.

Reactivities of fluorocarbon gases from decomposed PTFE with WO_3. Based on the IR spectroscopy results in the section above, PTFE decomposition at 500 °C initially produces C_2F_4 and possibly :CF_2, which are then converted to *c*-C_4F_8, C_3F_6, and *i*-C_4F_8. Although the direct reaction between the :CF_2 and WO_3 is plausible, it has been previously reported to have a short lifetime (0.1 sec at most).[80] However, the present configuration of WO_3 and PTFE in individual Ni boats makes the occurrence of this reaction highly unlikely. This is further substantiated by the *in situ* IR spectrum (Figure 2(b)), which clearly demonstrates that the reductive fluorination of WO_3 involves C_2F_4 as a main reaction species and not :CF_2. Even so, the decomposition of PTFE at 650, 700, and 750 °C has been previously reported to form *c*-C_4F_8 and C_3F_6 in the span of several seconds.[46] Thus, investigating the contribution of *c*-C_4F_8, C_3F_6, and *i*-C_4F_8 components in the present reductive fluorination would be pivotal to clearly depict the underlying reaction mechanisms.

In order to determine the reactions between the *c*-C_4F_8, C_3F_6, and *i*-C_4F_8 species and WO_3, the one-step reaction was divided into two steps wherein the PTFE-decomposition gas was cooled to 25 °C in a first step and reacted with WO_3 in a second step (F/W = 8.00), as illustrated by the schematic in Figure 3(a). In this configuration, the PTFE-decomposition gas was prepared by decomposing PTFE at 500 °C for 12 h and cooling it

to 25 °C overnight. In the second reaction step, WO_3 reacted with the PTFE-decomposition gas at 500 °C for 36 h.

As shown in Figure 3(b), the XRD pattern of the two-step reaction product was compared to the patterns obtained from pristine WO_3 and the one-step reaction product (same as Figure S8(d) and S10) to ascertain the semblances between their structures. The two-step reaction product manifests a pattern identical to the one-step reaction product – an indication that it also embodies the ReO_3-type cubic phase. This observation further evinces that some, if not all, of the *c*-C_4F_8, C_3F_6, and *i*-C_4F_8 also contribute to the reductive fluorination of WO_3 in a similar manner as C_2F_4.

The involvement of the PTFE-decomposition species in the two-step reaction was investigated through the IR spectroscopy of the residual gas obtained after the reaction. Figure 3(c) shows the IR spectrum of the two-step reaction residual gas alongside spectra of the PTFE-decomposition gas obtained and cooled in the absence of WO_3 (same as Figure 2(a-ii)) and the one-step reaction residual gas (500 °C, 36 h, and F/W = 8.00 in Table 1). A comparison between the IR spectra from the two-step reaction residual gas (Figure 3(c-ii)) and the one-step reaction residual gas (Figure 3(c-iii)) indicates that the reactions are nearly identical. Further investigation of the spectra in Figures 3(c-i) and 3(c-ii) reveals that the absorption bands assigned to *i*-C_4F_8 (1751 cm^{-1}) disappeared while

those ascribed to C_3F_6 (1795 cm^{-1}) became significantly weaker after the two-step reaction. On the other hand, the intensity of the bands assigned to *c*-C_4F_8 (*i.e.,* 962 and 569 cm^{-1}) notably remained stable before and after the two-step reaction. These results indicate that the C_3F_6 and *i*-C_4F_8 contributed to the reductive fluorination reaction at 500 °C, whereas the *c*-C_4F_8 remained inactive throughout the process. Additionally, the disappearance of the *i*-C_4F_8 bands after the two-step reaction affirms that *i*-C_4F_8 has a higher reactivity to WO_3 than C_3F_6.

Besides the fluorocarbon components of the two-step reaction residual gas, the IR spectrum also manifested bands assigned to the bending, and asymmetric stretching modes of CO_2 are found at 669 and 2350 cm^{-1},[82,83] alongside bands assigned to the stretching mode of CO around 2120 and 2170 cm^{-1}.[83,84] It should be pointed out that although previous works have reported the formation of CO_2 during reactions involving PTFE and metal oxides such as CuO, V_2O_5, and Fe_2O_3, the occurrence of CO has only been reported in a few cases, and has not even been proposed for the case of WO_3 to date.[52] However, the present study reveals that CO is formed even during the one-step reaction at 450 °C, which results in a product with a high oxygen content and low fluorination degree (see Figure S14 for IR spectrum of the residual gas after the one-step reaction at 450 °C for 36 h with F/W = 3.56). This indicates that CO does not generate as

a result of the decreasing O species in $WO_{3-x}F_x$ during the fluorination reactions but is instead generated concurrently with CO_2 throughout the reaction process

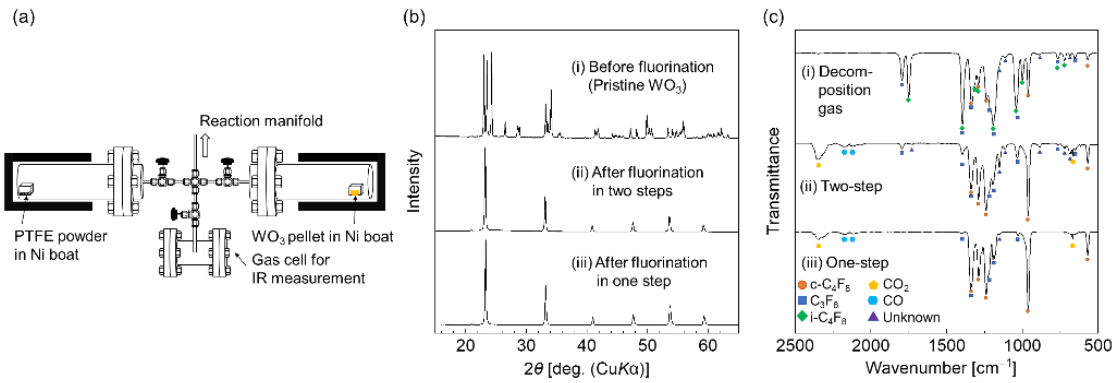

Figure 3. (a) Schematic of the two-step reaction between WO_3 and PTFE. The PTFE-decomposition gas obtained at 500 °C was cooled to 25 °C in the left reactor and transferred to the right reactor containing WO_3 for reaction at 500 °C. (b) XRD patterns of (i) pristine WO_3 and those after fluorination in (ii) the two steps, and (iii) the one step under the reaction temperature of 500 °C, and reaction hours of 36 h, and F/W = 8.00. (c) Infrared spectra of PTFE-decomposition gases before and after reaction. (i) PTFE-decomposition gas at 500 °C measured after cooling to 25 °C in the absence of WO_3, (ii) the residual gas after the two-step reaction of (i) with WO_3 (Figure 3(a)), and (iii) the residual gas after the one-step reaction with WO_3 (Figure 1(a)).

Reaction mechanisms of fluorocarbon gases from decomposed PTFE with WO_3. The formation of CO_2 and CO from C_2F_4, C_3F_6, and *i*-C_4F_8 evinces that the reaction induced the cleavage of carbon-carbon bonds in the C_2F_4, C_3F_6, and *i*-C_4F_8 species. Comparing the molecular structure of *c*-C_4F_8 with those of C_2F_4, C_3F_6, and *i*-C_4F_8, it is also justifiable to consider that the C=C bonds were not only cleaved but also involved with their reactivity. The cleavage of the C=C bond in C_2F_4, C_3F_6, and *i*-C_4F_8 ($R_1R_2C{=}CF_2$ (R_1, R_2 = F or CF_3)) forms $:CF_2$, C_2F_4, and C_3F_6, respectively. Therefore, $:CF_2$ formation can be considered to occur as a "knock-on effect " from the other components. Considering that the release of $:CF_2$ from C_2F_4, C_3F_6, and *i*-C_4F_8 under vacuum is thermodynamically unfavorable (see Figure S15 and Table S7 for the calculated Gibbs energies of the $:CF_2$ dissociation reactions from C_2F_4, C_3F_6, and *i*-C_4F_8 by a DFT method (B3LYP)), the interaction between the gas components and the WO_3 surface can be postulated to aid in the C=C bond cleavage and the concomitant $:CF_2$ formation. Difluorocarbene is notably more stable in the singlet state than in the triplet state, unlike its $:CH_2$ carbene equivalent, due to the π-donation from the F atoms to the divalent carbon atom. (see Figure S16 for the calculated structures of $:CF_2$ in the singlet and triplet states and their total energies).[85,86] It should also be pointed out that the formation of $:CF_2$ carbene is a known

decomposition product of CF_2-containing species such as HCF_2Cl and $ClCF_2COONa$ as well as C_2F_4, and can be used to introduce the CF_2 group to organic compounds.[85,87]

In the context of $:CF_2$ reactivity with $WO_{3-x}F_x$, the CO_2 and CO confirmed after the reactions are deemed to result from the simultaneous defluorination and oxidation of $:CF_2$. As such, the formation of CO_2 and CO is presumed to directly result from the reaction between $:CF_2$ and $WO_{3-x}F_x$, and not indirectly from the oxidation of CO and carbon by $WO_{3-x}F_x$. This is corroborated by previous works, which reported that the oxidation of CO and carbon by WO_3 cannot proceed at low temperatures of 450–550 °C.[88,89] The ratios of CO_2 and CO were estimated using their band intensities in the IR spectra after the reactions at 500 °C. The resulting ratios of CO_2 and CO were found to be closely comparable regardless of the reaction duration or F/W ratios applied (see Figure S17 and Table S8 for partial-pressure ratios of CO_2 and CO after the reactions at 500 °C).[90] Equation (1) below prescribes the CO_2 formation process during the reactions:

$$\mathrm{WO_3} + \frac{x}{2}\ \mathrm{:CF_2} \rightarrow \mathrm{WO_{3-x}F_x} + \frac{x}{2}\ \mathrm{CO_2}\uparrow \qquad (1)$$

This reaction corresponds to the reductive fluorination (2O–2F exchange), which provides a mixed oxidation state of W(VI) and W(V) in the $WO_{3-x}F_x$ (x is the F content

in the final product). On the other hand, the CO formation reaction is exemplified by Equation (2) below:

$$\mathrm{WO_3} + n :\mathrm{CF_2} \rightarrow \mathrm{WO_{3-n}F_{2n}}\uparrow + n\ \mathrm{CO}\uparrow \tag{2}$$

This reaction is a substitutive fluorination (O–2F exchange) which does not entail a change in the oxidation state of W. Here, n denotes the number of O atoms substituted. Alternatively, the CO formation can be rationalized by the reaction between $WO_{3-a}F_a$ and $:CF_2$, which also results in a phase separation involving W(VI) species ($WO_{3-n}F_{2n}$) and W(VI)-W(V) mixed species ($WO_{3-a'}F_{a'}$), as shown in Equation (3) (see Supporting Information for detailed coefficients and compositions of this equation):

$$\mathrm{WO_{3-a}F_a} + h :\mathrm{CF_2} \rightarrow k\ \mathrm{WO_{3-a'}F_{a'}} + l\ \mathrm{WO_{3-n}F_{2n}}\uparrow + m\ \mathrm{CO}\uparrow \tag{3}$$

Here, a and a' are the F contents in the intermediate compounds during the reaction in Equations (1) ($a < a' < x$). Since the resulting W(VI) species, $WO_{3-n}F_{2n}$, is volatile, it is promptly dissipated from the vicinity of the sample, thus increasing the fluorination

degree of the remaining solid sample and indirectly contributing to the reductive fluorination.

The sublimated W(VI) species are most likely WO_2F_2 and WOF_4, given their significant vapor pressures at the present reaction temperatures. Accordingly, the color of the sublimed compounds was noted to change from white or blue to yellow upon contact with air indicative of their hydrolysis to WO_3 (see Figure S13 for photos of the lid of the Ni reactor after the reaction at 500 °C for 36 h with F/W = 12.00). Moreover, it is the sublimation of W(VI) species during the CO-formation reaction, and not the sublimation of $WO_{3-x}F_x$, that provides a more plausible rationale for the decrease in weight observed in the reactions that yielded $WO_{3-x}F_x$ products with low x values (Table 1 and Figure 1 (c)). This is justified by the decreases in weight observed even in the reactions that produced $WO_{3-x}F_x$ with low x values such as 0.03 and 0.17 (Entries 1 and 2 in Table 1), although $WO_{3-x}F_x$ with x values below 0.4 are expected to have low vapor pressures given that $WO_{3-x}F_x$ with the x values at 0.4 is obtainable at 500 °C.

A broader look at the byproducts formed under different reaction conditions reveals that the carbon byproduct is only present in products obtained under severe reaction conditions (see Figure 1(c) and Table 1 for the correlation between reaction conditions and C_C). This suggests that carbon is only formed alongside CO_2 and CO during the

defluorination of :CF_2 in the presence of $WO_{3-x}F_x$ with deficient amounts of oxygen; after fluorination has progressed beyond a certain degree. This reaction process is expressed as Equation (4) below (see Supporting Information for detailed coefficients and compositions of this equation):

$$\mathrm{WO_{3-a}F_a} + p\ \mathrm{:CF_2} \rightarrow q\ \ \mathrm{WO_{3-a''}F_{a''}}\ \ + r\ \ \mathrm{C} + s\ \ \mathrm{WO_{3-n}F_{2n}} \uparrow \qquad (4)$$

Here, a'' is the F content in the product of the reaction in Equation (4) ($a'' < a < x$). The formation of the sublimable W(VI) species of $WO_{3-n}F_{2n}$ along with carbon highlighted in this chemical equation is in line with the trends observed in Table 1 and Figure 1(c), where increases in C_C values correspond with significant decreases in R_w values. In the same way, the carbon-formation reaction is seen to cause a decrease in the x values of $WO_{3-x}F_x$. This suggests that the x values of the $WO_{3-x}F_x$ in Figure 1 (c) and the concomitant partial sublimation from $WO_{3-x}F_x$ could not exceed a certain limit despite the continuous formation of CO_2 and CO during reactions.

For a deeper comprehension of the reaction process, the C=C bond strengths of C_2F_4, C_3F_6, and *i*-C_4F_8 were ascertained through quantum mechanical calculations at the B3LYP/6-311+G(d) and MP2/6-311+G(d) levels to determine their :CF_2 dissociation

capabilities. The calculated bond orders, bond lengths, and wavenumber of C=C bonds of C_2F_4, C_3F_6, and *i*-C_4F_8 are shown in Table 3 alongside those of C_2H_4, 2-*cis*-C_4F_8, 2-*trans*-C_4F_8, 1-C_4F_8 for comparison. The table also shows the energy gap of C_4F_8 olefin isomers with respect to *i*-C_4F_8. Here, the C_2F_4 is seen to have a lower C=C bond order than C_2H_4 – in agreement with the large interaction between the lone pair of fluorine and the antibonding π-orbital of the C=C bond.[91-93] The C=C bond order of C_3F_6 is lower than that of C_2F_4 as a result of the negative hyperconjugation of the resonance structure when CF_3 is introduced.[94] The bond order of *i*-C_4F_8 is further lower than that of C_3F_6 due to the second CF_3 group, in agreement with the lower wavenumber of the C=C stretching mode of *i*-C_4F_8 compared to C_3F_6 (see Figure 3(c) and Table 3 for experimental and computational results, respectively). Based on the theoretical data presented here, the higher reactivity of *i*-C_4F_8 towards $WO_{3-x}F_x$ in comparison to that of C_3F_6 (Figures 3(c-i) and (c-ii)) can be attributed to the weaker C=C bond of *i*-C_4F_8. Conversely, the bond orders of *cis*-2-C_4F_8 and *trans*-2-C_4F_8 are larger than those of C_3F_6 and even C_2F_4 due to the different positions of the additional CF_3 group. This trend results from the negative hyperconjugation in *cis*-2-C_4F_8 and *trans*-2-C_4F_8, which form carbocationic units that are stabilized by only single F atoms. The bond orders of 1-C_4F_8 and C_3F_6 are similar, corresponding to the similarities in their molecular structures except for CF_3 substituted

with C_2F_5 in 1-C_4F_8. Among the C_4F_8 olefin isomers highlighted in the table, *i*-C_4F_8 is shown to have the weakest C=C bond. Besides, the calculated energy gaps ΔE in Table 3 reveal that *i*-C_4F_8 formation is thermodynamically the most favorable among the C_4F_8 olefin isomers highlighted. In light of this favorable *i*-C_4F_8 formation, the PTFE decomposition gas does not contain the other C_4F_8 olefin isomers (see Figure 2(a) for the IR spectra of the PTFE decomposition gases).

Table 3. Summary of C=C bond parameters of C_2H_4 and fluoroolefin species and energy gaps of C_4F_8 isomers with respect to *i*-C_4F_8 calculated at B3LYP/6-311+G(d,p) and MP2/6-311+G(d,p)

	Molecule	C_2H_4 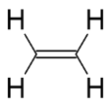	C_2F_4 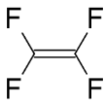	C_3F_6 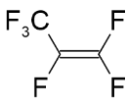	*i*-C_4F_8 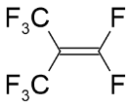	2-*cis*-C_4F_8 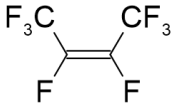	2-*trans*-C_4F_8 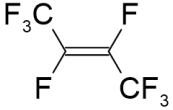	1-C_4F_8 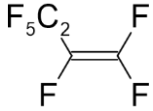
DFT (B3LYP)	C=C bond order	2.049	1.733	1.723	1.713	1.764	1.765	1.721
	C=C bond length (Å)	1.329	1.322	1.330	1.334	1.333	1.332	1.331
	Wavenumber for C=C [a] (cm^{-1})	(1684)	(1909)	1824	1766	1765	(1777)	1816
	ΔE [b] (kJ mol^{-1})	–	–	–	0	44.2	40.6	72.2
MP2	C=C bond order	2.040	1.806	1.787	1.753	1.832	1.833	1.7842
	C=C bond length (Å)	1.339	1.328	1.336	1.340	1.341	1.341	1.338
	Wavenumber for C=C [a] (cm^{-1})	(1675)	(1922)	1843	1795	1768	(1784)	1833
	ΔE [b] (kJ·mol^{-1})	–	–	–	0	55.0	52.8	84.5

[a]Wavenumbers in bracket indicate the vibration is IR inactive, [b]Energy gap from *i*-C_4F_8

Solid-solid reaction between WO_3 and $WO_{3-x}F_x$. Until this juncture, the present results and discussion have extensively mentioned that the fluorination of WO_3 occurs as a gas-solid reaction that involves gaseous *i*-C_4F_8, C_3F_6, and C_2F_4 to form CO_2 and CO. According to a previous study, the degree of fluorination is dependent on the metal oxide used. For instance, the fluorination of some oxides such as ZnO and Co_3O_4 only occurred on the surface, whereas other metal oxides such as CuO and V_2O_5 underwent bulk fluorination.[52] Although the reaction in this study is instigated on the WO_3 surface, fluorination was observed throughout the bulk of WO_3. This suggests the possible occurrence of F^- and O^{2-} diffusion within WO_3 during the reaction at around 500 °C. To verify this phenomenon, WO_3 and $WO_{2.64}F_{0.36}$ powders (synthesized at 500 °C for a reaction time of 36 h and F/W of 6.00, Table 1) were pelletized in a weight ratio of 90:10 and heated at 500 °C for 24 h. The schematic of this solid-solid reaction and the XRD pattern of the reaction product is provided in Figure 4(a). The XRD pattern of the solid-solid reaction product is provided alongside those of the starting WO_3 and $WO_{2.64}F_{0.36}$ (Figure 4(b)). After the reaction, the diffraction peaks of WO_3 are observed to completely disappear, resulting in a new diffraction pattern that is somewhat similar to that of $WO_{2.64}F_{0.36}$. Although the reaction product is not a single phase, it sufficiently demonstrates that F^- and O^{2-} diffusion occurs at 500 °C even in solid state, further

promoting the fluorination of WO_3.

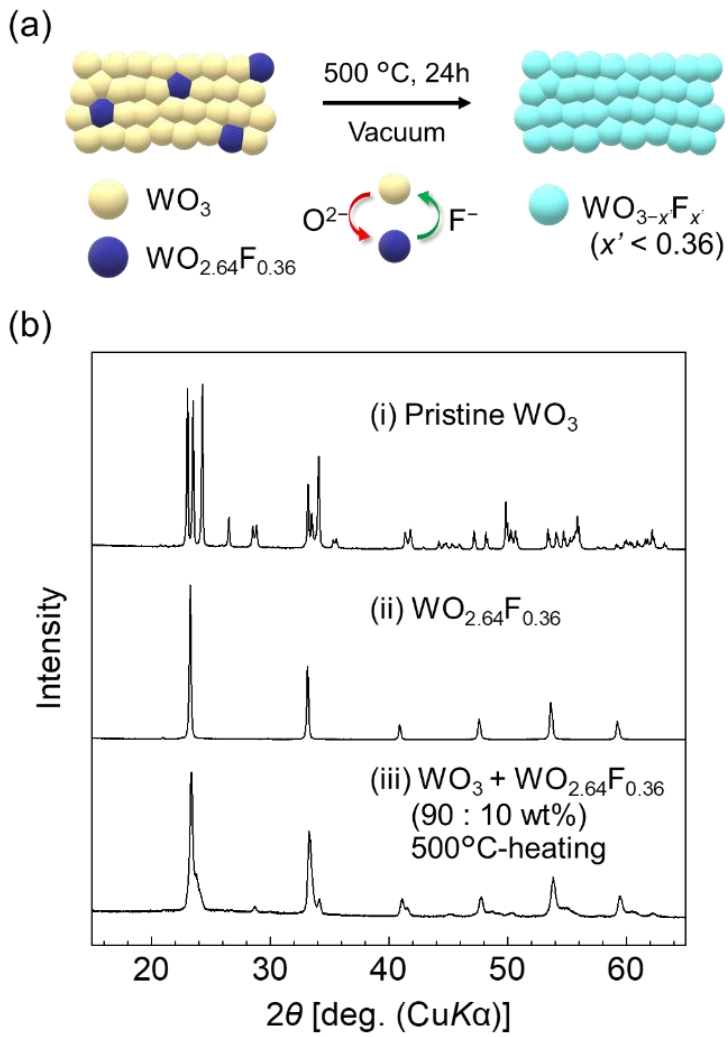

Figure 4. (a) Schematic of the solid-solid reaction between WO_3 and $WO_{2.64}F_{0.36}$. (b) XRD patterns of (i) pristine WO_3, (ii) $WO_{2.64}F_{0.36}$ (synthesized at 500 °C for 36 h with the F/W ratio of 6.00), and (iii) the product of the reaction between WO_3 and $WO_{2.64}F_{0.36}$ (90:10 wt%) at 500 °C for 24 h under vacuum (pelletized for solid-solid reaction).

Figure 5 illustrates a summary of the reaction mechanism between WO_3 and PTFE-decomposition gases. As shown, the decomposition of PTFE at high temperatures produces four different gaseous species: C_2F_4, C_3F_6, *i*-C_4F_8, and *c*-C_4F_8. The interaction between the C_2F_4, C_3F_6, and *i*-C_4F_8 and the surface of WO_3 results in the formation of $:CF_2$, which in turn induces reductive fluorination by exchanging the oxygen in WO_3 with fluorine. During the reaction $:CF_2$ carbene is also converted to CO via a O–2F exchange accompanied by sublimation of fluorine-containing W(VI) compounds and CO_2 is formed via a 2O–2F exchange during the reaction. The F^- ion in the solid phase further diffuses from the surface to the bulk of WO_3 by substituting O^{2-} eventually reaching a steady state of $WO_{3-x}F_x$.

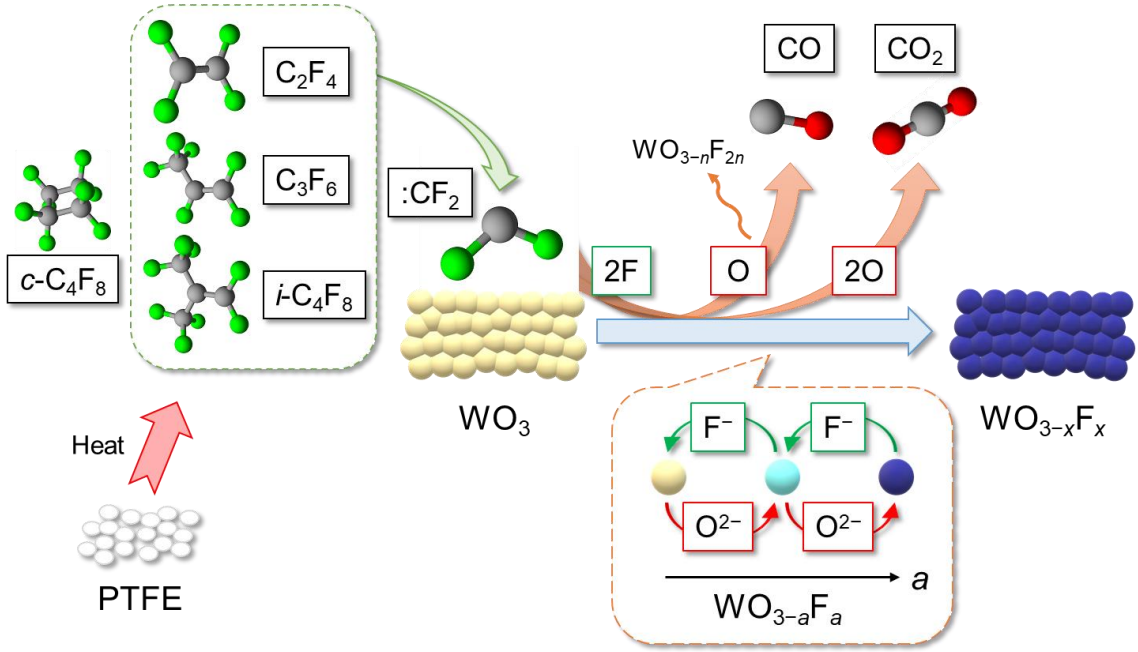

Figure 5 Schematic of the reaction mechanism for the reductive fluorination of WO_3 by PTFE-decomposition gas.

4. CONCLUSIONS

The present study investigates the mechanisms behind the reductive fluorination reaction between WO_3 and PTFE-decomposition gases to optimize reaction conditions, identify reactive chemical species, and ascertain the pertinent gas-solid and solid-solid reaction paths. The reactions are conducted in nickel reactors as an alternative to quartz reactors to avoid reactions between PTFE-decomposition gas and quartz.

The reaction conditions were explored under one-step process, and appropriate reaction temperature, duration, and PTFE quantity (F/W) were found to be essential to obtain cubic $WO_{3-x}F_x$ because formation of amorphous carbon byproduct and sublimation of fluorine-containing W(VI) compounds occurred at high temperature (550 °C under F/W = 3.56 and 36 h) and high PTFE quantity (F/W ≥ 10.00 under 500 °C and 36 h). The analysis of the PTFE decomposition gases performed at 25 °C and 500 °C (*in situ*) after the decomposition at 500 °C under vacuum confirmed the generation of C_2F_4 at the first step and its conversion into *c*-C_4F_8, C_3F_6, and *i*-C_4F_8. The two-step reaction process revealed that C_3F_6 and *i*-C_4F_8 are also reactive species in addition to C_2F_4. The reductive fluorination reaction was induced by $:CF_2$ formed by the cleavage of the C=C bond in the C_2F_4, C_3F_6, and *i*-C_4F_8 upon contact with the surface of WO_3. The reaction between WO_3 and $:CF_2$ notably occurred via two mechanisms: (i) an O–2F exchange reaction that leads

to CO formation accompanied by the sublimation of fluorine-containing W(VI) compounds; and (ii) a 2O–2F exchange that produces CO_2. Quantum chemical calculations showed that *i*-C_4F_8 has a weaker C=C bond than C_3F_6, which is consistent with the higher reactivity of *i*-C_4F_8 than that of C_3F_6 confirmed in the two-step reaction. The formation of *i*-C_4F_8 is thermodynamically the most favorable compared with that of the other C_4F_8 fluoroolefin isomers, thereby rationalizing the presence of only *i*-C_4F_8 among the C_4F_8 isomers in the PTFE decomposition gases. The diffusion process of O^{2-} and F^- in the solid state was also confirmed by a direct reaction between WO_3 and $WO_{2.64}F_{0.36}$ at 500 °C.

The reaction model proposed here provides an unprecedented insight into the reductive fluorination of metal oxides using PTFE. Although the optimal conditions and rate-determining steps are dependent on the metal oxide species, this report presents an fundamental framework for future explorations. Further, we expect this study to result in interest in reductive fluorination mechanisms involving different oxide materials and other fluoropolymers for more valuable insights.

SUPPORTING INFORMATION.

The Supporting Information is available free of charge at DOI: xx. Details on some PTFE-related reactions; infrared and XPS spectra, XRD pattern and related structural analyses, and thermogravimetric curve of reaction products; photos of the reactor; thermodynamic and structural data of theoretical calculations (PDF).

ACKNOWLEDGEMENTS. This work was financially supported by the JSPS KAKENHI Grant Numbers 19H04695 (K. M.), 19H04688 (D. H.), and 20K15177 (K. T.). The authors thank Prof. Shigeyuki Yamada of Kyoto Institute of Technology for the discussion on the stability of fluoroolefins.

REFERENCES

(1) Greiner, M. T.; Chai, L.; Helander, M. G.; Tang, W.-M.; Lu, Z.-H. Transition metal oxide work functions: the influence of cation oxidation state and oxygen vacancies. *Adv. Funct. Mater.* **2012**, *22*, 4557-4568.

(2) Sathiya, M.; Rousse, G.; Ramesha, K.; Laisa, C. P.; Vezin, H.; Sougrati, M. T.; Doublet, M. L.; Foix, D.; Gonbeau, D.; Walker, W.; et al. Reversible anionic redox chemistry in high-capacity layered-oxide electrodes. *Nat. Mater.* **2013**, *12*, 827-835.

(3) Meyer, J.; Hamwi, S.; Kröger, M.; Kowalsky, W.; Riedl, T.; Kahn, A. Transition metal oxides for organic electronics: energetics, device physics and applications. *Adv. Mater.* **2012**, *24*, 5408-5427.

(4) Kageyama, H.; Hayashi, K.; Maeda, K.; Attfield, J. P.; Hiroi, Z.; Rondinelli, J. M.; Poeppelmeier, K. R. Expanding frontiers in materials chemistry and physics with multiple anions. *Nature Communications* **2018**, *9*, 772.

(5) Ebbinghaus, S. G.; Abicht, H.-P.; Dronskowski, R.; Müller, T.; Reller, A.; Weidenkaff, A. Perovskite-related oxynitrides – Recent developments in synthesis, characterisation and investigations of physical properties. *Prog. Solid State Chem.* **2009**, *37*, 173-205.

(6) Tsujimoto, Y.; Yamaura, K.; Takayama-Muromachi, E. Oxyfluoride chemistry of

layered perovskite compounds. *Appl. Sci.* **2012**, *2*, 206-219.

(7) Pei, Y.; Shi, X.; LaLonde, A.; Wang, H.; Chen, L.; Snyder, G. J. Convergence of electronic bands for high performance bulk thermoelectrics. *Nature* **2011**, *473*, 66-69.

(8) Li, Y.-Y.; Wang, W.-J.; Wang, H.; Lin, H.; Wu, L.-M. Mixed-anion inorganic compounds: a favorable candidate for infrared nonlinear optical materials. *Cryst. Growth Des.* **2019**, *19*, 4172-4192.

(9) Xiao, J.-R.; Yang, S.-H.; Feng, F.; Xue, H.-G.; Guo, S.-P. A review of the structural chemistry and physical properties of metal chalcogenide halides. *Coord. Chem. Rev.* **2017**, *347*, 23-47.

(10) Clemens, O.; Slater, P. R. Topochemical modifications of mixed metal oxide compounds by low-temperature fluorination routes. *Rev. Inorg. Chem.* **2013**, *33*, 105-117.

(11) Francesconi, M. G.; Greaves, C. Anion substitutions and insertions in copper oxide superconductors. *Supercond. Sci. Technol.* **1997**, *10*, A29-A37.

(12) McCabe, E. E.; Greaves, C. Fluorine insertion reactions into pre-formed metal oxides. *J. Fluorine Chem.* **2007**, *128*, 448-458.

(13) Hirai, D.; Sawai, O.; Nunoura, T.; Hiroi, Z. Facile synthetic route to transition metal oxyfluorides via reactions between metal oxides and PTFE. *J. Fluorine Chem.* **2018**, *209*, 43-48.

(14) Hirai, D.; Climent-Pascual, E.; Cava, R. J. Superconductivity in $WO_{2.6}F_{0.4}$ synthesized by reaction of WO_3 with teflon. *Phys. Rev. B* **2011**, *84*, 174519.

(15) Kobayashi, Y.; Tian, M.; Eguchi, M.; Mallouk, T. E. Ion-exchangeable, electronically conducting layered perovskite oxyfluorides. *J. Am. Chem. Soc.* **2009**, *131*, 9849-9855.

(16) Ai-Mamouri, M.; Edwards, P. P.; Greaves, C.; Slaski, M. Synthesis and superconducting properties of the strontium copper oxy-fluoride $Sr_2CuO_2F_{2+\delta}$. *Nature* **1994**, *369*, 382-384.

(17) Slater, P. R. Poly(vinylidene fluoride) as a reagent for the synthesis of K_2NiF_4-related inorganic oxide fluorides. *J. Fluorine Chem.* **2002**, *117*, 43-45.

(18) Pinlac, R. A. F.; Stern, C. L.; Poeppelmeier, K. R. New layered oxide-fluoride perovskites: $KNaNbOF_5$ and $KNaMO_2F_4$ (M = Mo^{6+}, W^{6+}). *Crystals* **2011**, *1*, 3-14.

(19) Troyanchuk, I. O.; Kasper, N. V.; Mantytskaya, O. S.; Shapovalova, E. F. High-pressure synthesis of some perovskite — Like compounds with a mixed anion type. *Mater. Res. Bull.* **1995**, *30*, 421-425.

(20) Katsumata, T.; Nakashima, M.; Umemoto, H.; Inaguma, Y. Synthesis of the novel perovskite-type oxyfluoride $PbScO_2F$ under high pressure and high temperature. *J. Solid State Chem.* **2008**, *181*, 2737-2740.

(21) Galasso, F.; Darby, W. Preparation, structure, and properties of K_2NbO_3F. *J. Phys.*

Chem. **1962**, *66*, 1318-1320.

(22) *Functionalized inorganic fluorides: synthesis, characterization & properties of nanostructured solids*, 1st ed.; Tressaud, A., Ed.; John Wiley & Sons: New Jersey, 2010.

(23) Lange, M. A.; Krysiak, Y.; Hartmann, J.; Dewald, G.; Cerretti, G.; Tahir, M. N.; Panthöfer, M.; Barton, B.; Reich, T.; Zeier, W. G.; et al. Solid state fluorination on the minute scale: synthesis of $WO_{3-x}F_x$ with photocatalytic activity. *Adv. Funct. Mater.* **2020**, *30*, 1909051.

(24) Lange, M. A.; Khan, I.; Opitz, P.; Hartmann, J.; Ashraf, M.; Qurashi, A.; Prädel, L.; Panthöfer, M.; Cossmer, A.; Pfeifer, J.; et al. A generalized method for high-speed fluorination of metal oxides by spark plasma sintering yields Ta_3O_7F and TaO_2F with high photocatalytic activity for oxygen evolution from water. *Adv. Mater.* **2021**, *33*, 2007434.

(25) Wang, J.; Shin, Y.; Gauquelin, N.; Yang, Y.; Lee, C.; Jannis, D.; Verbeeck, J.; Rondinelli, J. M.; May, S. J. Physical properties of epitaxial $SrMnO_{2.5-\delta}F_\gamma$ oxyfluoride films. *J. Phys.: Condens. Matter* **2019**, *31*, 365602.

(26) Wen, T.; Zhou, Y.; Yang, B.; Wang, Y. Controllable Synthesis, Polymorphism and Structure-Dependent Photoluminescence Properties of Europium Oxyfluorides. *Eur. J. Inorg. Chem.* **2017**, *2017*, 5121-5126.

(27) Tsujimoto, Y.; Yamaura, K.; Hayashi, N.; Kodama, K.; Igawa, N.; Matsushita, Y.;

Katsuya, Y.; Shirako, Y.; Akaogi, M.; Takayama-Muromachi, E. Topotactic synthesis and crystal structure of a highly fluorinated ruddlesden–popper-type iron oxide, $Sr_3Fe_2O_{5+x}F_{2-x}$ ($x \approx 0.44$). *Chem. Mater.* **2011**, *23*, 3652-3658.

(28) Wen, T.; Zhou, Y.; Guo, Y.; Zhao, C.; Yang, B.; Wang, Y. Color-tunable and single-band red upconversion luminescence from rare-earth doped Vernier phase ytterbium oxyfluoride nanoparticles. *J. Mater. Chem. C* **2016**, *4*, 684-690.

(29) Wen, T.; Ding, R.; Zhou, Y.; Si, Y.; Yang, B.; Wang, Y. Polymorphism of erbium oxyfluoride: selective synthesis, crystal structure, and phase-dependent upconversion luminescence. *Eur. J. Inorg. Chem.* **2017**, *2017*, 3849-3854.

(30) Wen, T.; Li, X.; Ning, D.; Yao, J.; Yang, B.; Wang, Y. Selective synthesis, polymorphism, reversible phase transition and structure-dependent optical functionalities of gadolinium oxyfluorides. *J. Mater. Chem. C* **2018**, *6*, 11007-11014.

(31) Clemens, O.; Haberkorn, R.; Slater, P. R.; Beck, H. P. Synthesis and characterisation of the $Sr_xBa_{1-x}FeO_{3-y}$-system and the fluorinated phases $Sr_xBa_{1-x}FeO_2F$. *Solid State Sci.* **2010**, *12*, 1455-1463.

(32) Clemens, O.; Kuhn, M.; Haberkorn, R. Synthesis and characterization of the $La_{1-x}Sr_xFeO_{3-\delta}$ system and the fluorinated phases $La_{1-x}Sr_xFeO_{3-x}F_x$. *J. Solid State Chem.* **2011**, *184*, 2870-2876.

(33) Moon, E. J.; Xie, Y.; Laird, E. D.; Keavney, D. J.; Li, C. Y.; May, S. J. Fluorination of epitaxial oxides: synthesis of perovskite oxyfluoride thin films. *J. Am. Chem. Soc.* **2014**, *136*, 2224-2227.

(34) Wissel, K.; Heldt, J.; Groszewicz, P. B.; Dasgupta, S.; Breitzke, H.; Donzelli, M.; Waidha, A. I.; Fortes, A. D.; Rohrer, J.; Slater, P. R.; et al. Topochemical fluorination of La_2NiO_{4+d}: unprecedented ordering of oxide and fluoride ions in $La_2NiO_3F_2$. *Inorg. Chem.* **2018**, *57*, 6549-6560.

(35) Juillerat, C. A.; Tsujimoto, Y.; Chikamatsu, A.; Masubuchi, Y.; Hasegawa, T.; Yamaura, K. Fluorination and reduction of $CaCrO_3$ by topochemical methods. *Dalton Trans.* **2020**, *49*, 1997-2003.

(36) Chikamatsu, A.; Kawahara, K.; Shiina, T.; Onozuka, T.; Katayama, T.; Hasegawa, T. Fabrication of fluorite-type fluoride $Ba_{0.5}Bi_{0.5}F_{2.5}$ thin films by fluorination of perovskite $BaBiO_3$ precursors with poly(vinylidene fluoride). *ACS Omega* **2018**, *3*, 13141-13145.

(37) Sleight, A. W. Tungsten and molybdenum oxyfluorides of the type $MO_{3-x}F_x$. *Inorg. Chem.* **1969**, *8*, 1764-1767.

(38) Reynolds, T. G.; Wold, A. Preparation and Properties of Tetragonal Tungsten Oxyfluoride Bronzes. *J. Solid State Chem.* **1973**, *6*, 565-568.

(39) Derrington, C. E.; Godek, W. S.; Castro, C. A.; Wold, A. Preparation and

photoelectrolytic behavior of the systems tungsten oxide (WO_{3-x}) and tungsten fluoride oxide ($WO_{3-x}F_x$). *Inorg. Chem.* **1978**, *17*, 977-980.

(40) Shein, I. R.; Ivanovskii, A. L. Ab initio probing of the electronic band structure and Fermi surface of fluorine-doped WO_3 as a novel low-T C superconductor. *JETP Lett.* **2012**, *95*, 66-69.

(41) Shein, I. R.; Ivanovskii, A. L. Effect of fluorine, nitrogen, and carbon impurities on the electronic and magnetic properties of WO_3. *Semiconductors* **2013**, *47*, 740-744.

(42) Pellegrini, C.; Glawe, H.; Sanna, A. Density functional theory of superconductivity in doped tungsten oxides. *Phys. Rev. Mater.* **2019**, *3*, 064804.

(43) Woodward, P. M.; Sleight, A. W.; Vogt, T. Ferroelectric tungsten trioxide. *J. Solid State Chem.* **1997**, *131*, 9-17.

(44) Vogt, T.; Woodward, P. M.; Hunter, B. A. The high-temperature phases of WO_3. *J. Solid State Chem.* **1999**, *144*, 209-215.

(45) Puts, G. J.; Crouse, P.; Ameduri, B. M. Polytetrafluoroethylene: synthesis and characterization of the original extreme polymer. *Chem. Rev.* **2019**, *119*, 1763-1805.

(46) Bezuidenhoudt, A.; Sonnendecker, P. W.; Crouse, P. L. Temperature and pressure effects on the product distribution of PTFE pyrolysis by means of qualitative, in-line FTIR analysis. *Polym. Degrad. Stab.* **2017**, *142*, 79-88.

(47) Poutsma, M. L. Chain elongation during thermolysis of tetrafluoroethylene and hexafluoropropylene: Modeling of mechanistic hypotheses and elucidation of data needs. *J. Anal. Appl. Pyrolysis* **2011**, *92*, 25-42.

(48) Simon, C. M.; Kaminsky, W. Chemical recycling of polytetrafluoroethylene by pyrolysis. *Polym. Degrad. Stab.* **1998**, *62*, 1-7.

(49) Odochian, L.; Moldoveanu, C.; Mocanu, A. M.; Carja, G. Contributions to the thermal degradation mechanism under nitrogen atmosphere of PTFE by TG-FTIR analysis. Influence of the additive nature. *Thermochim. Acta* **2011**, *526*, 205-212.

(50) Bhadury, P. S.; Singh, S.; Sharma, M.; Palit, M. Flash pyrolysis of polytetrafluoroethylene (teflon) in a quartz assembly. *J. Anal. Appl. Pyrolysis* **2007**, *78*, 288-290.

(51) Puts, G. J.; Crouse, P. L. The influence of inorganic materials on the pyrolysis of polytetrafluoroethylene. Part 1: The sulfates and fluorides of Al, Zn, Cu, Ni, Co, Fe and Mn. *J. Fluorine Chem.* **2014**, *168*, 260-267.

(52) Puts, G. J.; Crouse, P. L. The influence of inorganic materials on the pyrolysis of polytetrafluoroethylene. Part 2: The common oxides of Al, Ga, In, Zn, Cu, Ni, Co, Fe, Mn, Cr, V, Zr and La. *J. Fluorine Chem.* **2014**, *168*, 9-15.

(53) van der Walt, I. J.; Neomagus, H. W. J. P.; Nel, J. T.; Bruinsma, O. S. L.; Crouse, P.

L. A kinetic expression for the pyrolytic decomposition of polytetrafluoroethylene. *J. Fluorine Chem.* **2008**, *129*, 314-318.

(54) Siegle, J. C.; Muus, L. T.; Lin, T.-P.; Larsen, H. A. The molecular structure of perfluorocarbon polymers. II. pyrolysis of polytetrafluoroethylene. *J. Polym. Sci. A* **1964**, *2*, 391-404.

(55) Conesa, J. A.; Font, R. Polytetrafluoroethylene decomposition in air and nitrogen. *Polym. Eng. Sci.* **2001**, *41*, 2137-2147.

(56) Lewis, E. E.; Naylor, M. A. Pyrolysis of Polytetrafluoroethylene. *J. Am. Chem. Soc.* **1947**, *69*, 1968-1970.

(57) Drennan, G. A.; Matula, R. A. The pyrolysis of tetrafluoroethylene. *J. Phys. Chem.* **1968**, *72*, 3462-3468.

(58) Atkinson, B.; Atkinson, V. A. The thermal decomposition of tetrafluoroethylene. *J. Chem. Soc.* **1957**, 2086-2094.

(59) Odochian, L.; Moldoveanu, C.; Maftei, D. TG–FTIR study on thermal degradation mechanism of PTFE under nitrogen atmosphere and in air. Influence of the grain size. *Thermochim. Acta* **2014**, *598*, 28-35.

(60) Arito, H.; Soda, R. Pyrolysis products of polytetrafluoroethylene and polyfluoroethylenepropylene with reference to inhalation toxicity. *Ann. Occup. Hyg.*

1977, *20*, 247-255.

(61) Jun, H. S.; Kim, K. N.; Park, K. Y.; Woo, S. I. Thermal degradation of polytetrafluoroethylene in flowing helium atmosphere I. degradation rate. *Korean J. Chem. Eng.* **1995**, *12*, 156-161.

(62) Jun, H. S.; Kim, K. N.; Park, K. Y.; Woo, S. I. Thermal degradation of polytetrafluoroethylene in flowing helium atmosphere II. product distribution and reaction mechanism. *Korean J. Chem. Eng.* **1995**, *12*, 183-187.

(63) Van Der Walt, I. J.; Bruinsma, O. S. L. Depolymerization of clean unfilled PTFE waste in a continuous process. *J. Appl. Polym. Sci.* **2006**, *102*, 2752-2759.

(64) Meissner, E.; Wróblewska, A.; Milchert, E. Technological parameters of pyrolysis of waste polytetrafluoroethylene. *Polym. Degrad. Stab.* **2004**, *83*, 163-172.

(65) Morisaki, S. Simultaneous thermogravimetry-mass spectrometry and pyrolysis—gas chromatography of fluorocarbon polymers. *Thermochim. Acta* **1978**, *25*, 171-183.

(66) Matsumoto, K.; Hagiwara, R. Elimination of AsF_3 from anhydrous HF using $AgFAsF_6$ as a mediator. *J. Fluorine Chem.* **2010**, *131*, 805-808.

(67) Ponikvar, M.; Stibilj, V.; Žemva, B. Daily dietary intake of fluoride by Slovenian Military based on analysis of total fluorine in total diet samples using fluoride ion selective electrode. *Food Chem.* **2007**, *103*, 369-374.

(68) Becke, A. D. Density-functional thermochemistry. III. The role of exact exchange. *J. Chem. Phys.* **1993**, *98*, 5648-5652.

(69) Møller, C.; Plesset, M. S. Note on an approximation treatment for many-electron systems. *Phys. Rev.* **1934**, *46*, 618-622.

(70) M. J. Frisch, G. W. T., H. B. Schlegel, G. E. Scuseria, M. A. Robb, J. R. Cheeseman, G. Scalmani, V. Barone, G. A. Petersson, H. Nakatsuji, X. Li, M. Caricato, A. V. Marenich, J. Bloino, B. G. Janesko, R. Gomperts, B. Mennucci, H. P. Hratchian, J. V. Ortiz, A. F. Izmaylov, J. L. Sonnenberg, D. Williams-Young, F. Ding, F. Lipparini, F. Egidi, J. Goings, B. Peng, A. Petrone, T. Henderson, D. Ranasinghe, V. G. Zakrzewski, J. Gao, N. Rega, G. Zheng, W. Liang, M. Hada, M. Ehara, K. Toyota, R. Fukuda, J. Hasegawa, M. Ishida, T. Nakajima, Y. Honda, O. Kitao, H. Nakai, T. Vreven, K. Throssell, J. A. Montgomery, Jr., J. E. Peralta, F. Ogliaro, M. J. Bearpark, J. J. Heyd, E. N. Brothers, K. N. Kudin, V. N. Staroverov, T. A. Keith, R. Kobayashi, J. Normand, K. Raghavachari, A. P. Rendell, J. C. Burant, S. S. Iyengar, J. Tomasi, M. Cossi, J. M. Millam, M. Klene, C. Adamo, R. Cammi, J. W. Ochterski, R. L. Martin, K. Morokuma, O. Farkas, J. B. Foresman, and D. J. Fox, *Gaussian 2016*; Gaussian, Inc.: Wallingford CT, 2016.

(71) Wiberg, K. B. Application of the pople-santry-segal CNDO method to the cyclopropylcarbinyl and cyclobutyl cation and to bicyclobutane. *Tetrahedron* **1968**, *24*,

1083-1096.

(72) Reed, A. E.; Weinstock, R. B.; Weinhold, F. Natural population analysis. *J. Chem. Phys.* **1985**, *83*, 735-746.

(73) Nelson, C. T.; Overzet, L. J.; Goeckner, M. J. Temperature dependence of the infrared absorption cross-sections of neutral species commonly found in fluorocarbon plasmas. *J. Vac. Sci. Technol. A* **2012**, *30*, 021305.

(74) Blake, T. A.; Glendening, E. D.; Sams, R. L.; Sharpe, S. W.; Xantheas, S. S. High-resolution infrared spectroscopy in the 1200−1300 cm^{-1} region and accurate theoretical estimates for the structure and ring-puckering barrier of perfluorocyclobutane. *J. Phys. Chem. A* **2007**, *111*, 11328-11341.

(75) Vasekova, E.; Drage, E. A.; Smith, K. M.; Mason, N. J. FTIR spectroscopy and radiative forcing of octafluorocyclobutane and octofluorocyclopentene. *J. Quant. Spectrosc. Radiat. Transfer* **2006**, *102*, 418-424.

(76) Ballard, J.; Knight, R. J.; Newnham, D. A. Infrared absorption cross-sections and integrated absorption intensities of perfluoroethane and cis-perfluorocyclobutane. *J. Quant. Spectrosc. Radiat. Transfer* **2000**, *66*, 199-212.

(77) Brice, T. J.; LaZerte, J. D.; Hals, L. J.; Pearlson, W. H. The preparation and some properties of the C_4F_8 olefins. *J. Am. Chem. Soc.* **1953**, *75*, 2698-2702.

(78) Bomse, D. S.; Berman, D. W.; Beauchamp, J. L. Energetics of the rearrangement of neutral and ionized perfluorocyclopropane to perfluoropropylene. Use of infrared multiphoton dissociation spectra to identify structural isomers of molecular ions. *J. Am. Chem. Soc.* **1981**, *103*, 3967-3971.

(79) Milella, A.; Palumbo, F.; Favia, P.; Cicala, G.; d'Agostino, R. Deposition mechanism of nanostructured thin films from tetrafluoroethylene glow discharges. *Pure Appl. Chem.* **2005**, *77*, 399-414.

(80) Burkholder, J. B.; Howard, C. J.; Hamilton, P. A. Fourier transform spectroscopy of the ν_1 and ν_3 fundamental bands of CF_2. *J. Mol. Spectrosc.* **1988**, *127*, 362-369.

(81) Cameron, M. R.; Kable, S. H.; Bacskay, G. B. The electronic spectroscopy of jet-cooled difluorocarbene (CF_2): The missing Ã-state stretching frequencies. *J. Chem. Phys.* **1995**, *103*, 4476-4483.

(82) Suzuki, I. General anharmonic force constants of carbon dioxide. *J. Mol. Spectrosc.* **1968**, *25*, 479-500.

(83) Klarenaar, B. L. M.; Engeln, R.; van den Bekerom, D. C. M.; van de Sanden, M. C. M.; Morillo-Candas, A. S.; Guaitella, O. Time evolution of vibrational temperatures in a CO_2 glow discharge measured with infrared absorption spectroscopy. *Plasma Sources Sci. Technol.* **2017**, *26*, 115008.

(84) Mantz, A. W.; Maillard, J. P.; Roh, W. B.; Narahari Rao, K. Ground state molecular constants of $^{12}C^{16}O$. *J. Mol. Spectrosc.* **1975**, *57*, 155-159.

(85) Brahms, D. L. S.; Dailey, W. P. Fluorinated carbenes. *Chem. Rev.* **1996**, *96*, 1585-1632.

(86) Carter, E. A.; Goddard, W. A. Correlation-consistent singlet–triplet gaps in substituted carbenes. *J. Chem. Phys.* **1988**, *88*, 1752-1763.

(87) Takayama, R.; Yamada, A.; Fuchibe, K.; Ichikawa, J. Synthesis of sulfanylated difluoroalkenes: electrophilic difluoromethylidenation of dithioesters with difluorocarbene. *Org. Lett.* **2017**, *19*, 5050-5053.

(88) Swift, G. A.; Koc, R. Tungsten powder from carbon coated WO_3 precursors. *J. Mater. Sci.* **2001**, *36*, 803-806.

(89) Mohammadzadeh Valendar, H.; Rezaie, H.; Samim, H.; Barati, M.; Razavizadeh, H. Reduction and carburization behavior of NiO–WO_3 mixtures by carbon monoxide. *Thermochim. Acta* **2014**, *590*, 210-218.

(90) Tan, T. L.; Lebron, G. B. Determination of carbon dioxide, carbon monoxide, and methane concentrations in cigarette smoke by Fourier transform infrared spectroscopy. *J. Chem. Educ.* **2012**, *89*, 383-386.

(91) Wang, S. Y.; Borden, W. T. Why is the .pi. bond in tetrafluoroethylene weaker than

that in ethylene? An ab initio investigation. *J. Am. Chem. Soc.* **1989**, *111*, 7282-7283.

(92) Uchimaru, T.; Tsuzuki, S.; Chen, L.; Mizukado, J. Computational investigation of π-bond strengths in fluorinated ethylenes. *J. Fluorine Chem.* **2017**, *194*, 33-39.

(93) Fukaya, H.; Hayakawa, Y.; Okamoto, H.; Ueno, K.; Otsuka, T. Theoretical study of disproportionation reaction of fluorinated ethylenes. *J. Fluorine Chem.* **2017**, *200*, 133-141.

(94) Exner, O.; Böhm, S. Negative hyperconjugation of some fluorine containing groups. *New J. Chem.* **2008**, *32*, 1449-1453.

Graphical Abstract (8.25 cm x 4.45 cm)

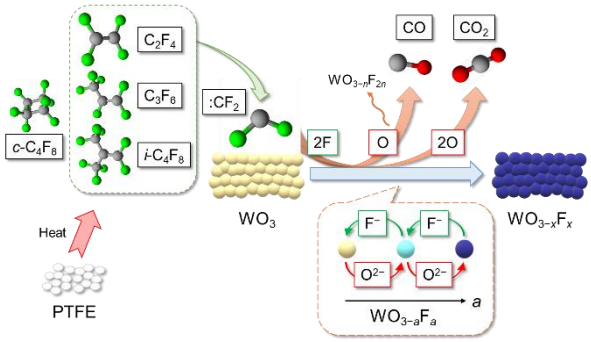

The reaction mechanisms behind the reductive fluorination of WO_3 using polytetrafluoroethylene have been explored under varied reaction conditions (temperature, duration, and F/W ratio) to suppress the formation of carbon byproducts, minimize the dissipation of fluorine-containing tungsten (VI) compounds, and achieve a high fluorine content.